

ANALYSIS OF ERUPTING SOLAR PROMINENCES IN TERMS OF AN UNDERLYING FLUX-ROPE CONFIGURATION

JONATHAN KRALL

Plasma Physics Division, Naval Research Laboratory, Washington, DC 20375-5346

AND

ALPHONSE C. STERLING¹

NASA Marshall Space Flight Center, SD50/Space Science Department, Huntsville, AL 35182

Received 2006 September 18; accepted 2007 March 21

ABSTRACT

Data from four solar prominence eruptions are analyzed so as to examine the flux-rope configuration at the onset of eruption and to test specific aspects of an analytic flux-rope model of solar eruptions. The model encompasses both prominence eruptions and coronal mass ejections (CMEs) as generic elements of a typical erupting flux-rope structure. The hypothesized relationship between prominence footpoint separation and prominence acceleration profile is examined, as is the hypothesized geometrical relationship between the prominence and the CME leading edge (LE). While the simple model does not account for some observed features, the prominence and “loop” (LE) data are shown to be consistent with both the geometrical model and the theoretical acceleration profile. This analysis further suggests that the onset of eruption is associated with a situation in which the underlying flux-rope geometry maximizes the outward magnetic “hoop” force.

Subject headings: Sun: coronal mass ejections (CMEs) — Sun: magnetic fields — Sun: prominences

1. INTRODUCTION

In recent years, the typical rim-cavity-prominence coronal mass ejection (CME) morphology (Illing & Hundhausen 1986; Hundhausen 1999) has been hypothesized to be the result of an underlying magnetic flux-rope geometry. This hypothesis has been applied to the description of prominences (Kuperus & Raadu 1974; van Ballegoijen & Martens 1989; Low & Hundhausen 1995; Kuijpers 1997; Schutgens 1997; Linker et al. 2001; Aulanier et al. 2002; Lionello et al. 2002; van Ballegoijen 2004), CMEs (Mouschovias & Poland 1978; Mikić & Linker 1994; Chen 1996; Wu et al. 1997; Lin et al. 1998), and to combined flux-rope/prominence/CME structures (Forbes 1990; Chen et al. 1997; Chen & Krall 2003; Gibson & Low 1998, 2000; Dere et al. 1999; Plunkett et al. 2000; Filippov & Den 2001; Yurchyshyn et al. 2001; Yurchyshyn 2002; Gibson et al. 2006).

While a number of prominence and CME events (Vršnak 1990; Vršnak et al. 1993; Plunkett et al. 2000; Srivastava et al. 2000; Ciaravella et al. 2000; Yurchyshyn et al. 2001) have been analyzed in terms of the flux-rope concept, and while prominence eruptions are strongly associated with observed CMEs (MacQueen 1985; Wilson & Hildner 1986; Bothmer & Schwenn 1994; Feynman & Martin 1995; Gilbert et al. 2000), it is only recently that testable (i.e., quantitative) hypotheses of the relationship between the prominence (if present), the CME (if present), and the underlying flux rope have emerged (Gibson & Low 1998; Chen & Krall 2003). Indeed, the hypothesis that prominences and CMEs are always part of an underlying flux-rope geometry is not well tested. Under this hypothesis, the flux-rope geometry presumably ties the CME to the prominence in all eruptive events in which both features are present. In this context we are motivated to study prominences because they can be observed in the near-Sun region and,

in many cases, on the solar disk. In particular, the locations of prominence footpoints, where the ends of a prominence contact the Sun, are often directly observable.

In this paper we reexamine the prominence and “coronal loop” observations of Sterling & Moore (2004a, 2004b, 2005) in terms of specific aspects of the theoretical framework of Chen & Krall (2003). In that framework, an underlying flux-rope magnetic structure, which cannot be directly observed, has an apex at height $Z(t)$ above the solar surface and fixed footpoints embedded in that surface, separated by a distance S_f . Chen & Krall (2003) implied specific quantitative relationships between $Z(t)$, the prominence height $Z_p(t)$, and the CME leading-edge height $Z_{LE}(t)$. Chen & Krall (2003) stated their geometrical hypotheses in order to make a connection between CME and prominence observations and their analysis of flux-rope acceleration. The primary result of that analysis is that the main acceleration phase of a flux-rope eruption occurs near the Sun, with the flux-rope acceleration profile d^2Z/dt^2 reaching its peak value at a height Z_{peak} , and with Z_{peak} being bounded by

$$S_f/2 < Z_{\text{peak}} < 3S_f/2. \quad (1)$$

This equation is obtained from equation (18) of Chen & Krall (2003) by substituting in their equations (13) and (17b) and setting their parameter $\chi = 2$ as stated in the text that precedes equation (18).

Chen & Krall (2003) presented a number of hypotheses that are testable using prominence and “coronal loop” observations of the type reported in Sterling & Moore (2004a, 2004b, 2005). One purpose of this paper is to analyze these events in terms of those hypotheses. A second aim of this paper is to examine the flux-rope conditions associated with the onset of eruption. These data are interesting because they clearly capture the eruption onset and because, in two cases, they include simultaneous prominence and “leading-edge” data. In those two cases the data allow a direct

¹ Current address: Japan Aerospace Exploration Agency (JAXA), Institute of Space and Astronautical Science (ISAS), Hinode Group, 3-1-1 Yoshinodai, Sagamihara, Kanagawa 229-8510.

test of the Chen & Krall (2003) assumption that R/a is approximately constant (see § 2.1), where R is the radius of curvature of the flux-rope axis and a is proportional to the width of the flux rope at its apex.

We note that analysis of prominence data in terms of a quantitative flux-rope model (or any quantitative model) presents two key difficulties. The first of these is that the observation of an optically thin three-dimensional structure via two-dimensional images from a single spacecraft introduces projection effects that cannot be resolved. Here we shall assume radial motion. However, observations of CMEs (Tripathi et al. 2004; Krall et al. 2006; Yurchyshyn et al. 2006) and their interplanetary counterparts (Webb et al. 2000; Krall et al. 2006; Yurchyshyn et al. 2006) show that deflections of order 10° away from radial motion are not uncommon.

The second difficulty is that the source regions for prominence and CME eruptions exhibit a wide variety of magnetic configurations. Beyond the fact that long filament channels seem to produce CMEs with large angular widths and high-field active regions seem to be associated with more energetic CMEs (MacQueen & Fisher 1983), little has been determined, and the significance of the source-region magnetic field configuration remains a matter of debate. In this study we focus on a theory that specifies analytical expressions relating observed quantities (heights of prominence and overlying CME or “loop” features) to a simple hypothesized magnetic structure. Here we focus on these central features and set aside, for now at least, questions related to the “opening” or “pushing aside” of overlying or nearby magnetic structures.

One might question the utility of such a simple model. In addition to testing and perhaps adding to the model under consideration, one of the aims of this study is to challenge others to produce similar quantitative tests of analytic and numerical models. This represents a challenge to both the modelers and to the observers.

Ultimately, a successful model will be one in which only parts of the overall prominence/field/CME structure need be observed in order to obtain a quantitative picture of the overall structure that is in some way useful. For example, the results of such near-Sun analyses might be used to generate inputs for a large-scale numerical model of the heliosphere.

The remainder of this paper proceeds as follows. In § 2 we review the theoretical framework of Chen & Krall (2003). In § 3 we describe the theoretical analysis of prominence observations in terms of that framework. In § 4 we analyze four specific events first reported by Sterling & Moore (2004a, 2004b, 2005). We close with a brief discussion in § 5.

2. A THEORETICAL FRAMEWORK FOR PROMINENCES AND CMES

We now review two specific aspects of the theoretical framework of Chen & Krall (2003): the flux-rope/prominence/CME geometry and the linear relationship between the acceleration-profile scale length and the distance separating the flux-rope magnetic footpoints. In a case where the acceleration profile is analyzed, these two theoretical constructs must be considered simultaneously. In particular, while the geometry of the underlying flux-rope magnetic structure can dictate the acceleration profile, it is the prominence and/or the CME that are actually observed.

2.1. Flux-Rope, Prominence, and CME Geometry

In Chen & Krall (2003), as in their prior studies, the near-surface erupting flux rope has a circular shape, with the flux-rope

axis apex height $Z(t)$ and flux-rope footpoint separation distance S_f being related to the radius of curvature $R(t)$ by (see, e.g., Fig. 1 of Chen 1996)

$$R = (Z^2 + S_f^2/4)/2Z. \quad (2)$$

This particular equation, which holds only if the axis of the flux rope traces out a circular arc, has been shown not to hold for apex heights above $2\text{--}3 R_\odot$; at greater heights the flux-rope axis can be approximated as an ellipse (Krall et al. 2006; Krall & St. Cyr 2006; Krall 2007). However, we follow Chen & Krall (2003), Krall et al. (2006), and Chen et al. (2006) by continuing to assume that the flux rope has a circular shape during the main acceleration phase, which takes place near the solar surface (Chen & Krall 2003).

As is typical, this hypothesized flux-rope structure has twisted fields. In the Chen & Krall (2003) framework, these fields are supported by an axial current, confined to a “current channel” of radius $a(t)$. Thus, the flux rope features an untwisted field line on its axis, increasing twist as one moves outward from the axis to the edge of the current channel, and highly twisted fields extending beyond the current channel (fields lie outside of the current channel just as fields lie outside of a current-carrying wire). Naturally, those highly twisted fields can support plasma (Krall & Chen 2005). Based on model-data comparisons for CME events (Chen et al. 1997, 2000; Krall et al. 2000, 2001), Chen & Krall (2003) have continued to assume that this plasma corresponds to the “bright rim” of the CME and that the CME outer edge lies at a distance $2a$ from the axis of the flux rope. Thus, the CME leading edge is at height

$$Z_{LE} = Z + 2a. \quad (3)$$

Similarly, Chen & Krall (2003) assumed that the relatively cool prominence material flows within the current channel, where the fields are most strongly connected to the chromospheric plasma that is the presumed source of this material. Further assuming, as others do (Kuperus & Raadu 1974; Antiochos et al. 1994; Filippov 1998; Aulanier et al. 1999; Karpen et al. 2003), that this material tends to collect in dips in the field lines, they postulate that prominence material settles at the lower edge of the current channel. The apex of the prominence is therefore located at height

$$Z_p = Z - a. \quad (4)$$

Because prominence end points are often visible on the solar disk, the separation between these points S_p is often observable; it is related to S_f by

$$S_p = S_f - 2a_0, \quad (5)$$

where a_0 is the current-channel radius at the footpoints. Like S_f and S_p , a_0 is assumed to be constant on the timescale of the eruption.

The relationships between Z , Z_p , and a are illustrated in Figure 1, which shows an image taken by the LASCO C2 telescope (Brueckner et al. 1998) of a CME event on 1998 June 2. This image, which corresponds to a flux-rope CME viewed axially, shows a nearly circular bright rim surrounding a low-density cavity (the leading edge of the rim is outside of the LASCO C2 field of view at this time). Very bright prominence material is evident, with the prominence apex apparently located on the inner edge of the bright rim below (Sunward of) the cavity. Ignoring

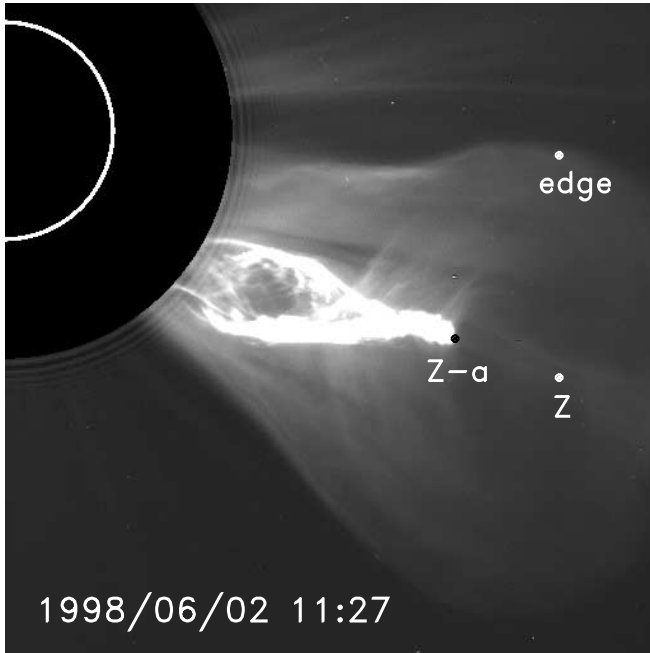


FIG. 1.—LASCO image from 1998 June 2 at 11:27 UT with flux-rope height Z and prominence height $Z - a$ indicated.

projection effects for the moment, we see that, if the center of the cavity is located at a height Z above the limb of the Sun, and if the radius of the cavity is a , then the outer edge of the bright rim outside the cavity lies at a distance $\simeq 2a$ from the center of the cavity, and the apex of the prominence has height $Z - a$. Later images from LASCO C3 show that these relationships persist as the CME continues to expand outward. While this event provides a clear illustration of the correspondence between the model prominence geometry and the model flux-rope geometry, it remains to be determined whether this placement of the prominence within the flux-rope CME geometry is as common as the flux-rope CME geometry has itself proven to be (Chen et al. 1997; Dere et al. 1999; Plunkett et al. 2000; Krall et al. 2001; Yurchyshyn et al. 2001; Ciaravella et al. 2003; Krall 2007).

For the purpose of analyzing a prominence observation in which $Z_p(t)$ and S_p are known, equations (2), (4), and (5) do not represent a closed set. In this case the unknowns are $Z(t)$, $a(t)$, $R(t)$, S_f , and a_0 ; two additional equations are needed. To address this, Chen & Krall (2003) further postulated that

$$a(t = 0) = a_0 \quad (6)$$

and

$$R/a = \text{constant} = \alpha \quad (7)$$

during the main acceleration phase, which is defined by $Z < 3S_f/2$. The idea that the preeruption flux rope has a constant thickness versus position along its length, equation (6), is supported by observations of coronal magnetic loops (Aschwanden et al. 2000; Klimchuk 2000).

Equation (7) is not directly supported by observations and is instead based on theoretical considerations. Specifically, analytical (Kumar & Rust 1996) and numerical (Chen 1996) solutions of flux-rope model equations show that, so long as the toroidal (axial) and poloidal (twisted) fluxes are conserved, which is equivalent to conserving helicity, the flux rope tends to expand in ac-

cordance with equation (7) (see eqs. [3]–[11] of Kumar & Rust 1996). Because equation (7) is valid only if the fluxes are conserved, this analysis is valid only if the flux changes during the main acceleration phase are small. In the model calculations of Chen & Krall (2003; see their Figs. 1–3), where a flux increase is specified, it is shown that the bulk of the flux increase occurs after the peak acceleration, suggesting equation (7) to be a reasonable approximation. The validity of this approximation is less clear for three-dimensional models in which the flux increases as a result of macroscopic reconnection (Amari et al. 2000; Tokman & Bellan 2002), as flux versus height (or time) curves have not been published for such cases.

To close the set of equations for the purpose of determining $Z(t)$, $a(t)$, $R(t)$, S_f , and a_0 from measurements of $Z_p(t)$ and S_p , α must be assigned a value. Chen & Krall (2003) used $\alpha = 2.5$ (see their § 4.1.4). In a later analysis, Chen et al. (2006) used $\alpha = 2.3 \pm 0.3$, the updated value being based on unpublished details of the flux-rope modeling results of Krall et al. (2001). In the analyses below, we shall use $\alpha = 2.3$ where needed.

2.2. Flux-Rope, Prominence, and CME Acceleration Profiles

As stated in § 1, Chen & Krall (2003) stated their geometrical hypotheses in order to make a connection between CME and prominence observations and their analysis of flux-rope acceleration. The primary result of that analysis is that the height of peak acceleration Z_{peak} is bounded by equation (1).

Equation (1) comes about by hypothesizing that the primary eruptive driving force is the magnetic “hoop force” (Shafranov 1966) acting in a curved flux rope that has fixed footpoints (Chen & Garren 1993; Lin et al. 1998). This hypothesis is typical of three-dimensional flux-rope models of CMEs (Chen & Garren 1993; Amari et al. 2000; Tokman & Bellan 2002; Roussev et al. 2003; Török & Kliem 2005). Simply stated, because the magnetic fields on the inner side of a curved flux rope are stronger than those on the outer side, there is a net outward-directed $\mathbf{J} \times \mathbf{B}$ force. This force increases with decreasing radius of curvature. For a circular flux rope with fixed footpoints, the minimum radius of curvature and therefore the maximum in the geometric factor in the force equation occurs when the flux rope is semicircular, with its height Z being $S_f/2$ (see Fig. 6 of Chen & Krall 2003). However, the net magnetic force is governed by other factors. In Chen & Krall (2003) this is expressed as (see their eq. [12c])

$$\frac{d^2Z}{dt^2} \sim k_R^2 \Phi_p^2 f_R, \quad (8)$$

where $k_R = [R \log(R/a_0)]^{-1}$ is a geometrical factor that peaks when the flux rope is semicircular and decreases thereafter, Φ_p is the flux associated with the twisted flux-rope field, and f_R is a factor related to the net magnetic force, including the action of the background magnetic field on the net current in the flux rope (see Chen & Krall 2003 for definitions of Φ_p and f_R).

Model calculations suggest that Φ_p and f_R typically increase with time. The flux Φ_p increases because current is driven along the flux rope (Chen & Garren 1993) or because macroscopic reconnection adds flux (Amari et al. 2000; Tokman & Bellan 2002). If the magnetic forces in the preeruption flux rope are approximately balanced, which is an excellent approximation for a coronal flux rope, $f_R \approx 0$ before the eruption and necessarily increases during the eruption. Observations of long-lived coronal cavities support this idea by suggesting that stable preeruption flux ropes are common (Gibson et al. 2006). The effect of the monotonically increasing Φ_p and f_R factors are to shift the peak acceleration height upward relative to the height at which the

flux-rope axis is semicircular. As the flux rope expands, however, the decreasing geometrical factor k_R dominates and the net force decreases. Thus, equation (1) bounds the height of peak acceleration Z_{peak} by $S_f/2$, the height Z where k_R is maximum, and $3S_f/2$, the height where k_R^2 decreases by approximately a factor of 4 relative to its peak. The relative importance of the geometrical and magnetic factors in equation (8) are illustrated in Figure 3 of Chen et al. (2006) which shows model results for eruptive events. The observational results reported in that same paper (see their Fig. 7) further verify that the peak acceleration occurs anywhere within the range specified in equation (1).

Because neither Z_{peak} nor S_f are directly observable, Chen & Krall (2003) imply that a practical test of equation (1) is provided by observations of the peak prominence acceleration height $Z_{p,\text{peak}}$, for which the equivalent relation is $S_f/2 < Z_{p,\text{peak}} + a_{\text{peak}} < 3S_f/2$. Here, a_{peak} is $a(t)$ at the time when $Z = Z_{\text{peak}}$ and, furthermore, $Z = Z_{\text{peak}}$ and $Z_p = Z_{p,\text{peak}}$ have been assumed to occur at the same time. To analyze CME measurements, Chen & Krall (2003) similarly assume that $Z = Z_{\text{peak}}$ and $Z_{\text{LE}} = Z_{\text{LE,peak}}$ occur at the same time.

The validity of equation (1) depends only on the existence of the flux rope prior to the time when its height Z exceeds $S_f/2$, on the flux rope being magnetically driven, on the footpoints being at fixed positions during the timescale of the eruption, and on the eruption-onset height being below the height range specified in equation (1). This relationship between the peak acceleration height and the footpoint separation distance is otherwise independent of the specifics of the drive mechanism.

3. ANALYSIS OF FLUX-ROPE GEOMETRY IN TERMS OF OBSERVABLE QUANTITIES

Chen & Krall (2003) present a number of relations that are testable using prominence and “coronal loop” observations of the type reported in Sterling & Moore (2004a, 2004b, 2005). Those papers examined, among other features, heights as functions of time of erupting prominences (filaments) and related features. These observations were chosen for our present analysis because they capture the onset of eruption in all cases and because they include simultaneous observations of both prominence and leading-edge features in two cases. The state of the underlying flux rope at the onset of eruption will be examined in each case. In cases where both the prominence and a leading-edge feature are observed simultaneously during acceleration, as with the two events of Sterling & Moore (2004b), equation (7) will be tested. In cases where the peak in the flux-rope acceleration profile can be inferred, equation (1) can also be tested, as has been done in Chen & Krall (2003) and Chen et al. (2006).

For the simple model under consideration here, the onset time will be taken to be the time of the latest image before the clear onset of eruption. We further take the onset time to be when both the velocity and acceleration curves show the beginning of a significant increase. This represents the end of the relatively quiescent preeruption period.

With the cadence of observations being 12 minutes in most cases (in the 1998 July 11 event it is 30 s), these time determinations are necessarily imprecise and, furthermore, differencing the data to obtain velocities and accelerations introduces large uncertainties. These affect the determination of the height and time of maximum acceleration. In some cases we smoothed the position data to mitigate noise in the velocity and acceleration curves. For each event discussed below, the onset time will be identified and the use of smoothing, if any, will be noted.

In addition, measured height-time data must be converted to actual heights above a source region in the photosphere by es-

timating and then removing the projection effects. In each case, radial motion is assumed with the source location taken to be the midpoint in the image between the two prominence footpoints, the locations of which we measure and report for each case below. The deprojected distance of the prominence apex from this source point is then taken to be the actual prominence height. Note that in Sterling & Moore (2004a, 2004b, 2005) the reported heights are measured along fiducial lines. The heights reported in the present study are deprojections of the heights from Sterling & Moore (2004a, 2004b, 2005) with an offset, H_{off} , added in each case to convert fiducial-line measurements to distances from the source point on the photosphere. To determine H_{off} for each feature, its position at the time of onset is measured and compared to the position obtained by deprojecting the corresponding height-time curve from Sterling & Moore (2004a, 2004b, 2005). Thus, $H_{\text{actual}} = H_{\text{measured}}/\sin(\theta) + H_{\text{off}}$, where H_{measured} is a value reported in Sterling & Moore (2004a, 2004b, 2005) and θ is the angle between the line of sight and the radial vector. For the prominence data, H_{off} is -4 , 40 , -180 , and -180 Mm, respectively, for each of the cases reported below. For the loop data, H_{off} is -160 and -90 Mm, respectively, for the 2000 February 26 and 2002 January 4 events. The process of deprojection can be problematic at early times. In particular, the model of the prominence as a simple arc, combined with the assumption of radial motion, suggests that the plane defined by the prominence arc should be everywhere normal to the solar surface. However, some images of prominences are not consistent with this picture (see, e.g., Fig. 1b of Sterling & Moore 2004b). Lacking a better approach, we shall nevertheless use the radial deprojection formula in all cases.

3.1. Analysis of a Prominence Acceleration Profile

We first consider the case where $Z_p(t)$ and S_p are known. Substituting equations (4), (5), and (7) into equation (2), we obtain

$$2\alpha a(Z_p + a) = (Z_p + a)^2 + (S_p + 2a_0)^2/4, \quad (9)$$

which provides a quadratic equation for $a(t)$. To obtain $a(t)$ from equation (9), however, a_0 must be determined. Considering $t = 0$ in equation (9), applying equation (6), and solving for a_0 , we find

$$a_0 = \frac{1}{4(\alpha - 1)} \left[S_p - 2(\alpha - 1)Z_{p,0} + \left\{ [2(\alpha - 1)Z_{p,0} - S_p]^2 + 2(\alpha - 1)(4Z_{p,0}^2 + S_p^2) \right\}^{1/2} \right], \quad (10)$$

where $Z_{p,0} = Z_p(t = 0)$. In practical terms, we take $t = 0$ to be the onset time. With a_0 determined from equation (10), we are now able to use equation (9) to obtain $a(t)$ from the measured values of $Z_p(t)$. Subsequently, using equation (4), $Z(t)$ is determined.

3.2. Analysis of a Prominence and “CME Loop” Height-Time Curves

In those cases where both $Z_{\text{LE}}(t)$ and $Z_p(t)$ can be determined from the observations, $Z(t)$ and $a(t)$ can be obtained rather simply from equations (3) and (4):

$$Z = (Z_{\text{LE}} + 2Z_p)/3, \quad (11)$$

$$a = (Z_{\text{LE}} - Z_p)/3. \quad (12)$$

However, to test equation (1), S_f must be determined from equations (5) and (6). In the instance that the Z_{LE} data include the

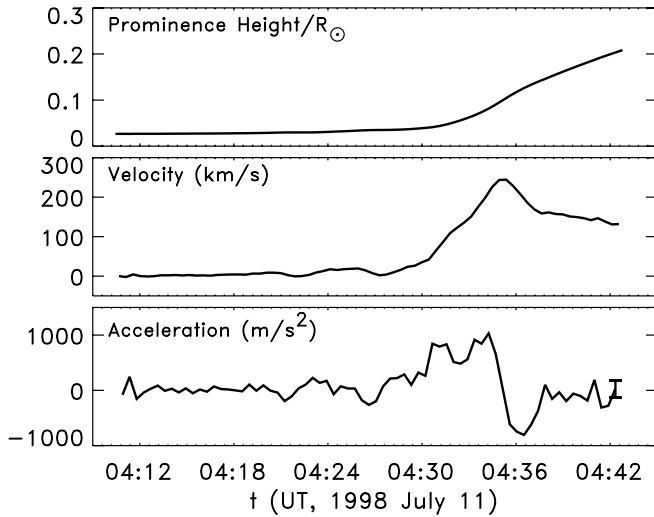


FIG. 2.—Height-time curve for the 1998 July 11 event (*top*). Heights have been deprojected to obtain the approximate actual height above the photosphere. Also plotted are velocity (*middle*) and acceleration (*bottom*).

preeruption quiescent state, a_0 can be obtained directly from equation (12). In this case, equation (7) is not used and can therefore be tested for validity, with $R(t)$ being obtained from equation (2). As above, we assume that the prominence footpoint separation S_p can be obtained from the prominence data and take $t = 0$ to be the onset time.

4. RESULTS: ANALYSIS OF PROMINENCE ERUPTIONS

4.1. 1998 July 11

This event is described in detail in Sterling & Moore (2005). Images of this event show a dark looplike prominence with fixed footpoints. Onset occurs at 4:28 UT, at which time the apex begins to move outward as the footpoints remain fixed. For example, Figure 1b of Sterling & Moore (2005), at 4:23 UT, shows two footpoints, one located at (800, -320), the other at (830, -340), these coordinates being given in arcseconds from disk center. This event is centered at approximately -25° south and 60° west. Recalling that $1'' = 0.73$ Mm at disk center, the actual prominence footpoint separation is approximately $22/\cos(60^\circ) = 44$ Mm in the x (longitude) direction and $15/\cos(25^\circ) = 17$ Mm in the y (latitude) direction. This gives $S_p = 47$ Mm in this case.

The deprojected ($\theta = 65^\circ$) height-time data for the prominence apex are plotted in Figure 2, where corresponding velocity and acceleration curves are also shown. The error level in the acceleration that results from uncertainties in the measurements is indicated at the last point plotted. We see that the prominence remains for a time at $Z_{p,0} = 0.028 R_\odot \simeq 20$ Mm, this value being measured from a image taken at 4:28 UT. We find peak acceleration at approximately 04:34 UT when the apex height is $Z_{p,\text{peak}} = 57$ Mm.

Turning now to the geometry at the time of eruption onset, equations (10) and (5) give $a_0 = 18$ Mm and $S_f = 79$ Mm, respectively. Thus, the flux rope is rather fat at onset, with height of the flux-rope axis being $Z_0 = 38$ Mm and the flux-rope thickness being $4a_0 = 72$ Mm. With a thickness of 72 Mm and a magnetic footpoint separation of 79 Mm, the two legs of the flux rope nearly abut each other. A diagram of this initial configuration is shown in Figure 3a, including the flux-rope axis (*dashed curve*) prominence (*hatched line*), and leading (LE) and trailing edges (*solid curves*) indicated. This rather fat flux-rope structure is qualitatively consistent with some models (Gibson & Low 1998; Chen et al. 2000)

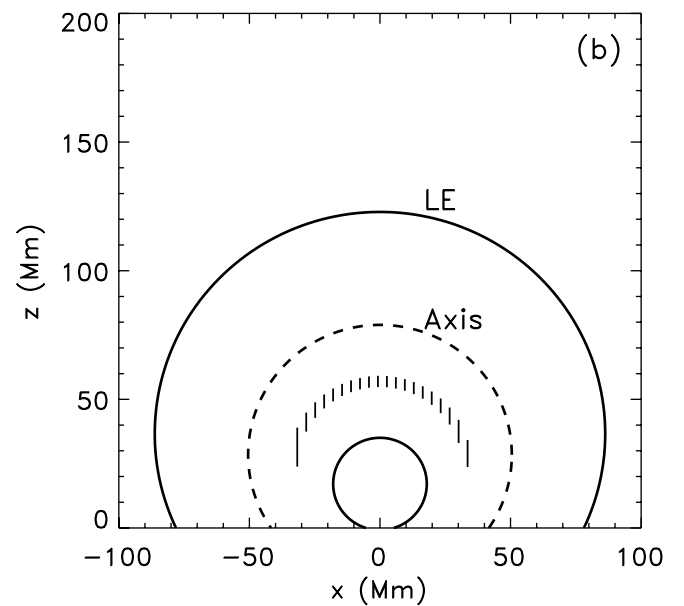
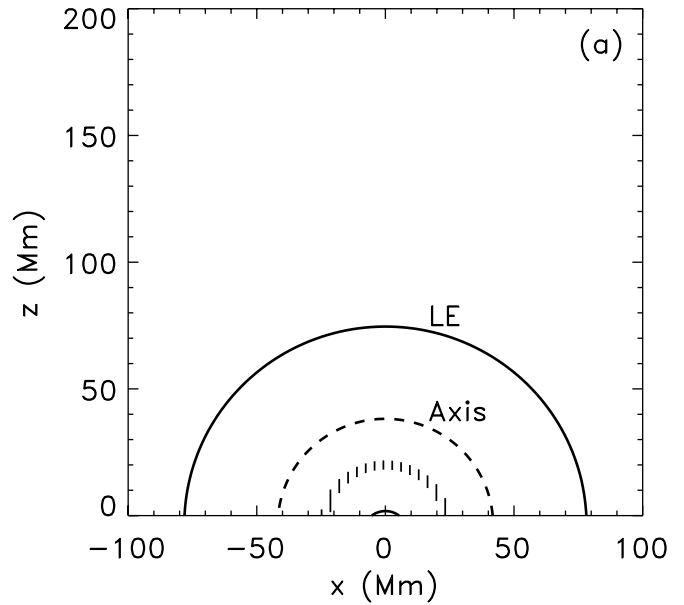


FIG. 3.—Diagrams of (a) the preeruption configuration and (b) the configuration at time of peak acceleration for the 1998 July 11 event. The outer curve indicates the leading edge, the dashed curve indicates the magnetic axis of the flux rope, the hatched line indicate prominence position, and the inner curve indicates the flux-rope trailing edge.

and is reminiscent of the concept that a CME is shaped like a “bubble” (see, e.g., Fig. 5.15b of Hundhausen 1999). We emphasize that the nearly semicircular onset configuration found in this case is not in conflict with Chen & Krall (2003), which does not explicitly address the conditions for onset. The fact that peak acceleration is expected to occur within the height range specified in equation (1) does seem to imply that onset should occur at a height $Z \leq S_f/2$. This situation is somewhat clouded by the abstract of Chen & Krall (2003), which states that “maximum acceleration is attained shortly after” $Z > S_f/2$. This seems to suggest a peak-acceleration height close to $S_f/2$ and, therefore, a somewhat lower onset height. However, Chen & Krall (2003) provide Z_{peak} and S_f for each of three events, with values of Z_{peak}/S_f ranging from 0.63 to 1.3. For these reasons we take the phrase “shortly

after” in Chen & Krall (2003) to mean “within the bounds of equation (1)” and conclude that an onset height of $S_f/2$ is allowable within the confines of their theory.

For this event, the measurements show a peak acceleration height that is consistent with equation (1). At 4:34 UT, the time of the observed peak acceleration, equations (9) and (4) give $a_{\text{peak}} = 22$ Mm and $Z_{\text{peak}} = 79$ Mm, respectively. However, with the exact peak in the acceleration profile being somewhat uncertain, Z_{peak} could be as low as 48 Mm [e.g., the local peak in $a(t)$ at 4:32 UT may correspond to the true peak]. In any case, equation (1) is satisfied, with $38 < Z_{\text{peak}} < 120$, these heights being in units of Mm. A diagram of the configuration at the time of peak acceleration is shown in Figure 3b, with the flux-rope axis (*dashed curve*), prominence (*hatched line*), and leading (LE) and trailing edges (*solid curves*) indicated.

There are a number of sources of error that may affect these results. Measurement errors, estimated to be of order 1 Mm in this case, lead to uncertainties in the deprojected velocities and accelerations; this error is indicated in the lower panel of Figure 2. The affect of these random measurement errors on the velocities and accelerations was alleviated somewhat by smoothing the data. The assumed value of α may also be in error, but any error in α tends to shift both S_f and Z_{peak} in a similar direction with the result that any agreement with equation (1) is not affected. Furthermore, overall heights are relatively insensitive to the value α ; a decrease in α by 20% increases Z_{peak} by 13%, and an increase in α by 20% decreases Z_{peak} by approximately 6%. Errors in S_p , which result from an assumed uncertainty of 5° in the source location, cause errors of only 3% in Z_{peak} . Errors in θ , the angle between the line of sight and the vector normal to the solar surface at the source, introduce systematic errors in deprojection. Because a typical active region is several degrees wide and because deflections of 10° away from radial motion are not uncommon (Webb et al. 2000; Tripathi et al. 2004; Krall et al. 2006; Yurchyshyn et al. 2006), we assume that $\delta\theta = 10^\circ$. With $\theta = 65^\circ \pm 10^\circ$ these systematic errors in the measured heights are of order 10%.

4.2. 1999 April 18

This event is described in detail in Sterling & Moore (2004a). Images of this event show a portion of a prominence (filament) erupting outward with the onset time being approximately 6:00 UT on 1999 April 18. Examination of Figure 1b of Sterling & Moore (2004a) shows that a portion of the filament is erupting with prominence material moving past the bright point labeled “bp” in the 07:25 UT image (see Fig. 1b of Sterling & Moore 2004a) at this time. Examination of this event suggests that the prominence footpoints were located at $(-280, 580)$ and $(-50, 470)$, these coordinates being given in arcseconds. With the event centered at approximately 30° north latitude and 5° west longitude, the actual prominence footpoint separation in latitude is approximately $170/\cos(30^\circ) = 200$ Mm. With no significant projection effect in the horizontal direction, we obtain $S_p = 220$ Mm.

The deprojected ($\theta = 30^\circ$) height-time data for the prominence apex are plotted in Figure 4, where corresponding velocity and acceleration curves are also shown. Here, the preeruption prominence has a height of $Z_{p,0} = 0.14 R_\odot \simeq 100$ Mm, which is rather small in comparison to S_p , implying a rather low-lying flux rope at the time of onset. Unfortunately, there is no sign of a peak in the acceleration curve at or before 07:10 UT, the latest time at which the prominence acceleration can be computed before it disappears from the Extreme-Ultraviolet Imaging Telescope (EIT; Delaboudinière et al. 1995) image sequence.

We now determine the model parameters for this case. Here, equations (10) and (5) give $a_0 = 85$ Mm and $S_f = 390$ Mm,

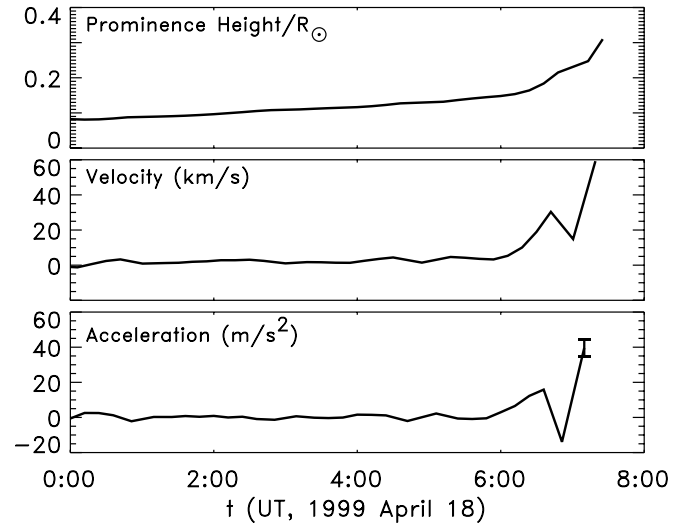


FIG. 4.—Height-time curve for the 1999 April 18 event (*top*). Heights have been deprojected to obtain the approximate actual height above the photosphere. Also plotted are velocity (*middle*) and acceleration (*bottom*).

respectively. The model, therefore, dictates that, at onset, the height of the flux-rope axis is $Z_0 = 180$ Mm. As in the 1998 July 11 case, the flux rope is rather fat. Also similar to the 1998 July 11 case, the value of Z_0 is close to that of $S_f/2$, so that the flux-rope axis, at onset, is approximately semicircular.

Because the peak in the acceleration profile is not observed, this event does not provide a test of equation (1), which dictates $190 \text{ Mm} < Z_{\text{peak}} < 580 \text{ Mm}$ in this case. At the time of the latest observed acceleration, we find $Z_p = 170$ Mm, $a = 90$ Mm, and $Z = 260$ Mm. As reported in the *SOHO* LASCO CME Catalog, LASCO C2 data show an average leading-edge acceleration (projected) of 12 m s^{-2} after 8:30 UT for this event. Even after deprojection, this acceleration is slightly weaker than that found for the prominence with the result that the data are not in conflict with the hypothesis that peak acceleration occurs within the bounds of equation (1).

As discussed above, there are a number of sources of error that might affect these quantitative results. Measurement errors are estimated to be of order 20 Mm in this case and, after smoothing of the data, lead to random uncertainties of order 5 m s^{-2} in the deprojected acceleration, as indicated in the lower panel of Fig. 4. Uncertainty in the value of S_p , estimated to be of order 20%, leads to an uncertainty of approximately 8% in Z . Perhaps the most significant source of error is the uncertainty in the angle θ between the viewer and the direction of motion. Because this event is relatively close to disk center, this systematic error can be large. For $\theta = 30^\circ \pm 10^\circ$, the error is of order 40%. With such large uncertainties in the absolute heights, all that can be said of this case is that (1) it does not present any obvious conflicts with our conclusions and (2) it illustrates the need for multiple observational points of view to constrain projection effects. In the near future, such observations will be provided by the Sun Earth Connection Coronal and Heliospheric Investigation (SECCHI) instrument suite on board each of the two the *Solar Terrestrial Relations Observatory* (STEREO) spacecraft (Howard et al. 2000).

4.3. 2000 February 26

This event is described in detail in Sterling & Moore (2004b). Images of this event show a tall quiescent prominence that begins to erupt at around 23:12 UT, which we take to be the onset time. An image of the prominence at 22:36 UT shows prominence

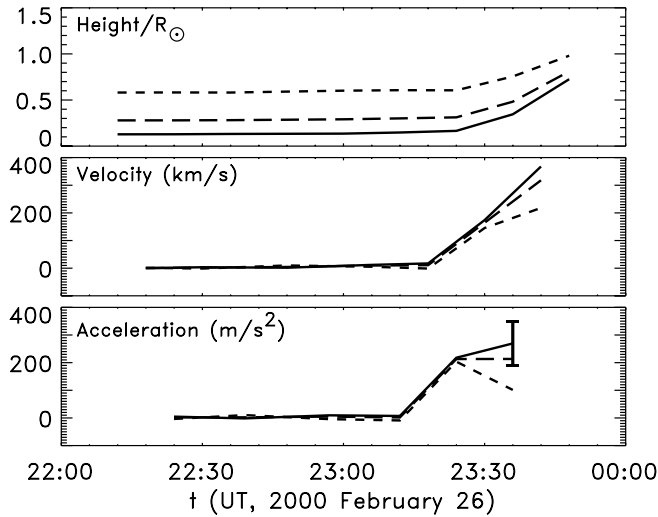


FIG. 5.—Height-time curves for the 2000 February 26 event (*top*). Heights for the prominence (*solid line*) and “loop” (*short-dashed line*) features have been deprojected to obtain the approximate actual heights above the photosphere. Also plotted are the theoretical result for the flux-rope centroid height Z (*long-dashed line*) and corresponding lines for the velocity (*middle*) and acceleration (*bottom*).

footpoints apparently located at $(-780, 580)$ and $(-700, 490)$, these coordinates being given in arcseconds (see Fig. 1*b* of Sterling & Moore 2004*b*, where the prominence is labeled “F”). With the event centered at approximately 25° north and 50° east, the actual prominence footpoint separation is approximately $58/\cos(50^\circ) = 90$ Mm in the x (longitude) direction and $66/\cos(25^\circ) = 73$ Mm in the y (latitude) direction. This gives $S_p = 120$ Mm in this case.

In this event, the EIT images show both prominence material and an outer loop feature, which we assume to correspond to the leading-edge bright rim that is often seen in coronagraph images. With $\theta = 55^\circ$, the deprojected height-time data for the prominence apex (*solid curve*) and loop feature (*short-dashed curve*) are shown in Figure 5. The theoretical result for the flux-rope centroid height Z from equation (11) is also shown (*long-dashed lines*), as are the corresponding velocity and acceleration curves. Sterling & Moore (2004*b*)’s study of this event also includes measurements of a “suspended” feature that appears to erupt along with the outer “loop” feature and the prominence. This additional feature, they believe, is embedded inside of the erupting filament cavity, and as such it has no direct counterpart in the simple theoretical framework under consideration (or, for that matter, any other published quantitative theory of prominence/CME structure).

At onset, the preeruption prominence and leading-edge heights are $Z_{p,0} = 0.14 R_\odot \simeq 99$ Mm and $Z_{LE,0} = 0.60 R_\odot \simeq 420$ Mm, respectively. With the measured values of S_p , $Z_p(t)$, and $Z_{LE}(t)$ as inputs, the theory describes an initial configuration with $S_f \simeq 330$ Mm, $Z_0 \simeq 190$ Mm, and $a_0 \simeq 100$ Mm. Figure 5 shows that the peak acceleration is not clearly determined. At 23:36 UT, the peak prominence acceleration (*solid line*) has not yet clearly occurred while the peak leading-edge acceleration (*short-dashed line*) seems to have passed. Theoretically, the net effect is that the acceleration of the flux-rope centroid (*long-dashed line*) seems to have leveled off. These data suggest $t_{\text{peak}} \simeq 23:36$ UT, so that $Z_{p,\text{peak}} = 240$ Mm, $Z_{LE,\text{peak}} = 530$ Mm, and $Z_{\text{peak}} \simeq 330$ Mm. At the very least, these values are lower bounds. This value of Z_{peak} is consistent with equation (1), which dictates $170 \text{ Mm} < Z_{\text{peak}} < 500 \text{ Mm}$. For this event, LASCO C2 data show deceleration in the motion of the CME leading edge as the event enters the

LASCO C2 field of view. This is consistent with our suggestion that the peak acceleration takes place at around $Z = 330$ Mm ($Z_{LE} = 530$ Mm).

With both prominence and leading-edge data, the sources of error in the heights are limited to measurement errors, of order 20 Mm (deprojected) in this case, and uncertainty in θ . In this event, the former leads to a random error of order 78 m s^{-2} in the prominence acceleration (indicated in the lower panel of Fig. 5) and the latter leads to a systematic deprojection error of order 15%. The estimate of the footpoint separation S_f is affected by these same errors, which are used to obtain a_0 via equation (12), and also by errors in S_p , estimated to be of order 25%. None of these errors is large enough to affect the apparent agreement between these data and equation (1).

With Z and a given by equations (11) and (12), we can obtain $R(t)$ from equation (2) and test the validity of equation (7). We find that α has an initial value of 1.6 and that it varies considerably in this case, increasing to a value 2.2 at 23:36 UT and jumping to 5.2 at 23:48 UT. This can be seen in the data plotted in Figure 5, where the Z_p and Z_{LE} curves are moving closer together rather than farther apart as would be expected if the expansion were self-similar.

Because the approximation of equation (7) does not hold throughout the eruption, an analysis based on the prominence data alone produces results that differ from those above. Specifically, with $\alpha = 2.3 = \text{constant}$, equations (10) and (5) give $a_0 = 50$ Mm and $S_f = 220$ Mm, respectively. With $Z_{p,0} = 100$ Mm from the data, equation (4) gives $Z_0 = 150$ Mm. Again taking $Z_{p,\text{peak}} \simeq 240$ Mm, equation (9) gives $a_{\text{peak}} \simeq 77$ Mm and $Z_{\text{peak}} \simeq 320$ Mm. Thus, the value of Z_{peak} that is obtained from analysis of the prominence data alone (320 Mm) is very close to that obtained above (330 Mm) through analysis of the combined prominence and loop data. This close agreement results, in part, from the fact that the value of α that is computed above from the Z_p and Z_{LE} data is in reasonable agreement with the value assumed here up until 23:36 UT, the peak acceleration time used above. In addition, these prominence-only results are only weakly sensitive to α ; variations in α within the observed range of 1.6–5.2 result in a maximum change in Z_{peak} of only 21%.

The flux rope in this case is not strictly in keeping with the flux-rope acceleration hypothesis, which leads one to expect that the eruption should begin at or below $Z = S_f/2$, when the flux rope is semicircular and the geometrical factor in the hoop force is maximum. Here, $Z_0 = 190 \text{ Mm} > S_f/2 = 170 \text{ Mm}$. However, the discrepancy is small enough and the uncertainties are large enough to keep this from being a clear counter example. In fact it is similar to the 1998 July 11 and 1999 April 18 events, in which $Z \simeq S_f/2$ at onset.

4.4. 2002 January 4

This event, like the 2000 February 26 eruption, is described in detail in Sterling & Moore (2004*b*) and includes measurements of both the prominence apex and an outer loop, apparently corresponding to the bright rim feature that is commonly seen in coronagraph images. Images of this event show a tall quiescent prominence, which begins to erupt at around 8:48 UT, which we take to be the onset time. An image of the preeruption prominence, shown in Figure 7*a* of Sterling & Moore (2004*b*) has prominence footpoints apparently located at $(-840, 400)$ and $(-820, 560)$, these coordinates being given in arcseconds. With the event centered at approximately 20° north and 80° east, the actual prominence footpoint separation is approximately $15/\cos(80^\circ) = 86$ Mm in the x (longitude) direction and $120/\cos(20^\circ) = 130$ Mm in the y (latitude) direction, so $S_p = 160$ Mm.

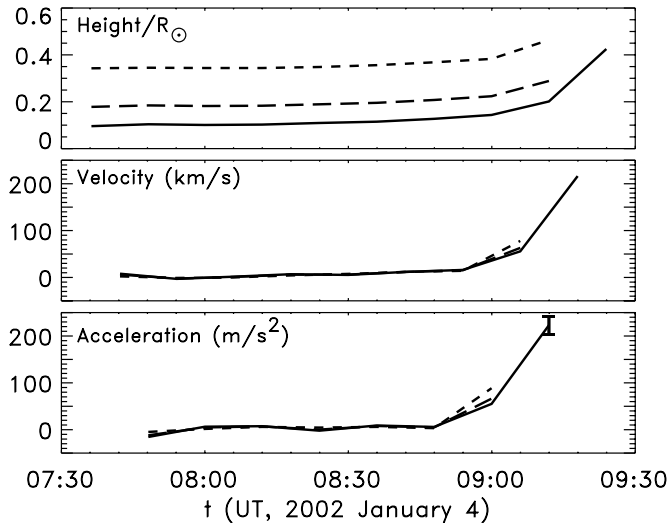


FIG. 6.—Height-time curves for the 2002 January 4 event (*top*). Heights for the prominence (*solid line*) and “loop” (*short-dashed line*) features have been deprojected to obtain the approximate actual heights above the photosphere. Also plotted are the theoretical result for the flux-rope centroid height Z (*long-dashed line*) and corresponding lines for the velocity (*middle*) and acceleration (*bottom*).

With $\theta = 80^\circ$, the deprojected height-time data for the prominence apex (*solid line*) and loop feature (*short-dashed line*) are shown in Figure 6. The theoretical result for the flux-rope centroid height Z from equation (11) is also shown (*long-dashed line*), as are the corresponding velocity and acceleration curves. At onset, the prominence and leading-edge heights are $Z_{p,0} = 0.10 R_\odot \simeq 70$ Mm and $Z_{LE,0} = 0.36 R_\odot \simeq 250$ Mm, respectively. With the measured values of S_p , $Z_p(t)$, and $Z_{LE}(t)$ as inputs, the theory describes a configuration with $S_f \simeq 280$ Mm, $Z_0 \simeq 130$ Mm, and $a_0 \simeq 60$ Mm.

As in the 1999 April 18 event, the peak in the acceleration profile is not observed, and this event does not provide a test of equation (1), which dictates $140 \text{ Mm} < Z_{\text{peak}} < 420 \text{ Mm}$. At 09:12 UT, the latest time at which the acceleration is determined, the prominence apex height is $Z_p = 140$ Mm, $Z_{LE} = 330$ Mm, and $Z \simeq 200$ Mm. For this event, LASCO C2 data show an average leading-edge deceleration (projected) of -26 m s^{-2} after 10:00 UT. That this deceleration is relatively weak in comparison to the peak acceleration shown in Figure 6 is consistent with, if not supportive of, the hypothesis that peak acceleration occurs within the bounds of equation (1).

Measurement errors in this case are estimated to be of order 5 Mm (deprojected) so that the uncertainty in the prominence acceleration is a similarly small 19 m s^{-2} , as indicated in Figure 6 (*lower panel*). With $\theta = 80^\circ \pm 10^\circ$, the deprojection error is only 5%. Errors in the footpoint separation S_f are affected by these same small measurement errors, as well as the larger estimated error of 30% in S_p resulting in an estimated error of 20% for S_f .

With deprojected height-time data for both Z_p and Z_{LE} , we can again use equations (11) and (12) to obtain Z and a . Obtaining $R(t)$ from equation (2), we find that α has an initial value of 2.4, within the range values reported in Chen et al. (2006) $\alpha = 2.3 \pm 0.3$. Because Z_{LE} is cut off just as the eruption is beginning, $\alpha(t)$ is also cut off. With this caveat in mind, we find that α does not vary significantly, remaining between 2.4 and 2.5 throughout.

Because α in this case is close to the value assumed in the analysis of prominence data alone, we find minimal variation between the analysis of the $Z_p(t)$ and $Z_{LE}(t)$ data versus analysis of the $Z_p(t)$

data alone. In the latter case, we find initial values $a_0 \simeq 60$ Mm, $Z_0 \simeq 130$ Mm, footpoint separation $S_f \simeq 280$ Mm, and at the latest time observed, $Z \simeq 210$ Mm. As in the events described above, we again find $Z_0 \simeq S_f/2$, suggesting that a configuration in which the geometrical factor in the hoop force is at its peak may be extremely favorable for eruption.

5. DISCUSSION

We have examined the height-time data for four prominence eruptions in terms of a specific model of an underlying flux rope, with the relationship between the prominence height Z_p and the leading-edge (“loop”) height Z_{LE} being prescribed in terms of the parameters of an underlying magnetic flux rope: height Z and characteristic width (current-channel radius) a . This model further dictates that the acceleration occur within a specific height range, given by equation (1). In the two cases where a significant portion of the initial acceleration associated with the eruption was observed, this acceleration occurs within this prescribed height range. However, the complete acceleration profile was only observed in one case.

In the two cases where both prominence and loop data were available, we were able to better examine the relationship between Z_p and Z_{LE} . Here we were able to test the approximation, made in Chen & Krall (2003) and Chen et al. (2006) and in the prominence-data analyses above, that $\alpha = R/a$ is approximately constant with a value close to 2.3 during the main acceleration phase of the eruption. We find that this approximation does not always hold, with α varying from 1.6 to 5.2 in the 2000 February 26 event. In the 2002 January 4 case, α did not vary significantly, remaining within $2.4 < \alpha < 2.5$ throughout. In both cases, however, analysis of combined $Z_p(t)$ and $Z_{LE}(t)$ data gave results very close to those obtained by analyzing the $Z_p(t)$ data alone. That is, analysis of the $Z_p(t)$ data in the context of this simple geometrical model provides an estimate of Z_{LE} that is in good agreement with the measured values. This occurred because the results are relatively insensitive to α and because α was within 20% of the assumed value during the period analyzed (just before until shortly after eruption) in both cases. Here it is important that we acknowledge that the measured structures typically appeared along side, or perhaps as an integral part of, regions of multiple magnetic loops. It is possible that these nearby magnetic fields influenced the evolution of R/a .

In all cases we analyzed the state of the flux rope at the time of eruption onset. While our study in no way comprehensively determines the necessary conditions for triggering an eruption, the results are suggestive. In Chen & Krall (2003), it is shown that, based on geometry alone, the outward $\mathbf{J} \times \mathbf{B}$ force that drives the eruption tends to peak at $Z = S_f/2$, where S_f is the separation between the footpoints of the magnetic flux rope. Additional factors, such as the background field that holds the preeruption flux rope in place or any process that might add flux to the flux rope as it erupts, tend to vary so as to make the height of peak acceleration higher than $Z = S_f/2$, as described by equation (1) (see eq. [18] of Chen & Krall 2003 and Fig. 7 of Chen et al. 2006). However, in all cases studied here, the onset height of the flux rope Z_0 , which is inferred from the measurements and the model geometrical relationships, was within 15% of the value of $S_f/2$.

In other words, the results suggest that the onset of eruption is associated with the situation in which the slowly increasing height of the flux-rope apex approaches $Z = S_f/2$, the height at which the geometrical factor in the outward hoop force is strongest. If

verified by further observations, this finding may lead to improved predictions of solar eruptions.

This work was supported by the Office of Naval Research and the National Aeronautics and Space Administration (DPR W-10106, LWS TRT Program, and NNH06AD56I, issued through the Office of Space Science). A. C. S. was supported by funding from NASA's Office of Space Science through the Solar Phys-

ics Supporting Research and Technology Program and the Sun-Earth Connection Guest Investigator Program. The *SOHO* LASCO data used here are produced by a consortium of the Naval Research Laboratory (USA), Max-Planck-Institut fuer Aeronomie (Germany), Laboratoire d'Astronomie (France), and the University of Birmingham (UK). The LASCO CME Catalog is generated and maintained at the CDAW Data Center by NASA and the Catholic University of America in cooperation with the Naval Research Laboratory. *SOHO* is a project of international cooperation between ESA and NASA.

REFERENCES

- Amari, T., Luciani, J. F., Mikić, Z., & Linker, J. 2000, *ApJ*, 529, L49
- Antiochos, S. K., Dahlburg, R. B., & Klimchuck, J. A. 1994, *ApJ*, 420, L41
- Aschwanden, M. J., Nightingale, R. W., & Alexander, D. 2000, *ApJ*, 541, 1059
- Aulanier, G., Démoulin, P., Mein, N., van Driel-Gesztelyi, L., Mein, P., & Schmieder, B. 1999, *A&A*, 342, 867
- Aulanier, G., DeVore, C. R., & Antiochos, S. K. 2002, *ApJ*, 567, L97
- Bothmer, V., & Schwenn, R. 1994, *Space Sci. Rev.*, 70, 215
- Brueckner, G. E., et al. 1998, *Geophys. Res. Lett.*, 25, 3019
- Chen, J. 1996, *J. Geophys. Res.*, 101, 27499
- Chen, J., & Garren, D. A. 1993, *Geophys. Res. Lett.*, 20, 2319
- Chen, J., & Krall, J. 2003, *J. Geophys. Res.*, 108, SSH 2-1
- Chen, J., Marqué, C., Vourlidas, A., Krall, J., & Schuck, P. W. 2006, *ApJ*, 649, 452
- Chen, J., et al. 1997, *ApJ*, 490, L191
- . 2000, *ApJ*, 533, 481
- Ciaravella, A., Raymond, J. C., van Ballegoijen, A., Strachan, L., Vourlidas, A., Li, J., Chen, J., & Panasyuk, A. 2003, *ApJ*, 597, 1118
- Ciaravella, A., et al. 2000, *ApJ*, 529, 575
- Delaboudinière, J.-P., et al. 1995, *Sol. Phys.*, 162, 291
- Dere, K. P., Brueckner, G. E., Howard, R. A., & Michels, D. J. 1999, *ApJ*, 516, 465
- Feynman, J., & Martin, S. F. 1995, *J. Geophys. Res.*, 100, 3355
- Filippov, B. P. 1998, *A&A*, 337, 883
- Filippov, B. P., & Den, O. G. 2001, *J. Geophys. Res.*, 106, 25177
- Forbes, T. G. 1990, *J. Geophys. Res.*, 95, 11919
- Gibson, S. E., Foster, D., Burkepile, J., de Toma, G., & Stanger, A. 2006, *ApJ*, 641, 590
- Gibson, S. E., & Low, B. C. 1998, *ApJ*, 493, 460
- . 2000, *J. Geophys. Res.*, 105, 18187
- Gilbert, H. R., Holzer, T. E., Burkepile, J. T., & Hundhausen, A. J. 2000, *ApJ*, 537, 503
- Howard, R. A., Moses, J. D., & Socker, D. G. 2000, *Proc. SPIE*, 4139, 259
- Hundhausen, A. J. 1999, in *The Many Faces of the Sun*, ed. K. Strong, et al. (New York: Springer), 143
- Illing, R. M. E., & Hundhausen, A. J. 1986, *J. Geophys. Res.*, 90, 10951
- Karpen, J. T., Antiochos, S. K., Klimchuck, J. A., & MacNeice, P. J. 2003, *ApJ*, 593, 1187
- Klimchuk, J. A. 2000, *Sol. Phys.*, 193, 53
- Krall, J. 2007, *ApJ*, 657, 559
- Krall, J., & Chen, J. 2005, *ApJ*, 628, 1046
- Krall, J., Chen, J., Duffin, R. T., Howard, R. A., & Thompson, B. J. 2001, *ApJ*, 562, 1045
- Krall, J., Chen, J., & Santoro, R. 2000, *ApJ*, 539, 964
- Krall, J., & St. Cyr, O. C. 2006, *ApJ*, 652, 1740
- Krall, J., Yurchyshyn, V. B., Slinker, S., Skoug, R. M., & Chen, J. 2006, *ApJ*, 642, 541
- Kuijpers, J. 1997, *ApJ*, 489, L201
- Kumar, A., & Rust, D. M. 1996, *J. Geophys. Res.*, 101, 15667
- Kuperus, M., & Raadu, M. A. 1974, *A&A*, 31, 189
- Lin, J., Forbes, T. G., Isenberg, P. A., Démoulin, P. 1998, *ApJ*, 504, 1006
- Linker, J., Lionello, R., Mikić, Z., & Amari, T. 2001, *J. Geophys. Res.*, 106, 25165
- Lionello, R., Mikić, Z., Linker, J. A., & Amari, T. 2002, *ApJ*, 581, 718
- Low, B. C., & Hundhausen, J. R. 1995, *ApJ*, 443, 818
- MacQueen, R. M. 1985, *Sol. Phys.*, 95, 359
- MacQueen, R. M., & Fisher, R. R. 1983, *Sol. Phys.*, 89, 89
- Mikić, Z., & Linker, J. A. 1994, *ApJ*, 430, 898
- Mouschovias, T. C., & Poland, A. I. 1978, *ApJ*, 220, 675
- Plunkett, S. P., et al. 2000, *Sol. Phys.*, 194, 371
- Roussev, I. I., Forbes, T. G., Gombosi, T. I., Sokolov, I. V., DeZeeuw, D. L., & Birn, J. 2003, *ApJ*, 588, L45
- Schutgens, N. A. J. 1997, *A&A*, 323, 969
- Shafranov, V. D. 1966, in *Reviews of Plasma Phys.*, vol. 2, ed. M. A. Leontovich (New York: Consultants Bureau), 103
- Srivastava, N., Schwenn, R., Inhester, B., Martin, S. F., & Hanaoka, Y. 2000, *ApJ*, 534, 468
- Sterling, A. C., & Moore, R. L. 2004a, *ApJ*, 602, 1024
- . 2004b, *ApJ*, 613, 1221
- . 2005, *ApJ*, 630, 1148
- Tokman, M., & Bellan, P. M. 2002, *ApJ*, 567, 1202
- Török, T., & Kliem, B. 2005, *ApJ*, 630, L97
- Tripathi, D., Bothmer, V., Solanki, S. K., Schwenn, R., Mierla, M., & Stenborg, G. 2004, in *IAU Symp. 223, Multi-Wavelength Investigations of Solar Activity*, ed. A. V. Stepanov, E. E. Benevolenskaya, & A. G. Kosovichev (Cambridge: Cambridge Univ. Press), 401
- van Ballegoijen, A. A. 2004, *ApJ*, 612, 519
- van Ballegoijen, A. A., & Martens, P. C. H. 1989, *ApJ*, 343, 971
- Vršnak, B. 1990, *Sol. Phys.*, 127, 129
- Vršnak, B., Rušđjak, V., Rimpolt, B., Roša, D., & Zlobec, P. 1993, *Sol. Phys.*, 146, 147
- Webb, D. F., Cliver, E. W., Crooker, N. U., St. Cyr, O. C., & Thompson, B. J. 2000, *J. Geophys. Res.*, 105, 7491
- Wilson, R. M., & Hildner, E. 1986, *J. Geophys. Res.*, 91, 5867
- Wu, S. T., Guo, W. P., & Dryer, M. 1997, *Sol. Phys.*, 170, 265
- Yurchyshyn, V., Liu, C., Abramenko, V., & Krall, J. 2006, *Sol. Phys.*, 239, 317
- Yurchyshyn, V. B. 2002, *ApJ*, 576, 493
- Yurchyshyn, V. B., Wang, H., Goode, P. R., & Deng, Y. 2001, *ApJ*, 563, 381